MATERIALS SCIENCE AND TECHNOLOGIES SERIES

SHAPE MEMORY ALLOYS

Manufacture, Properties and Applications

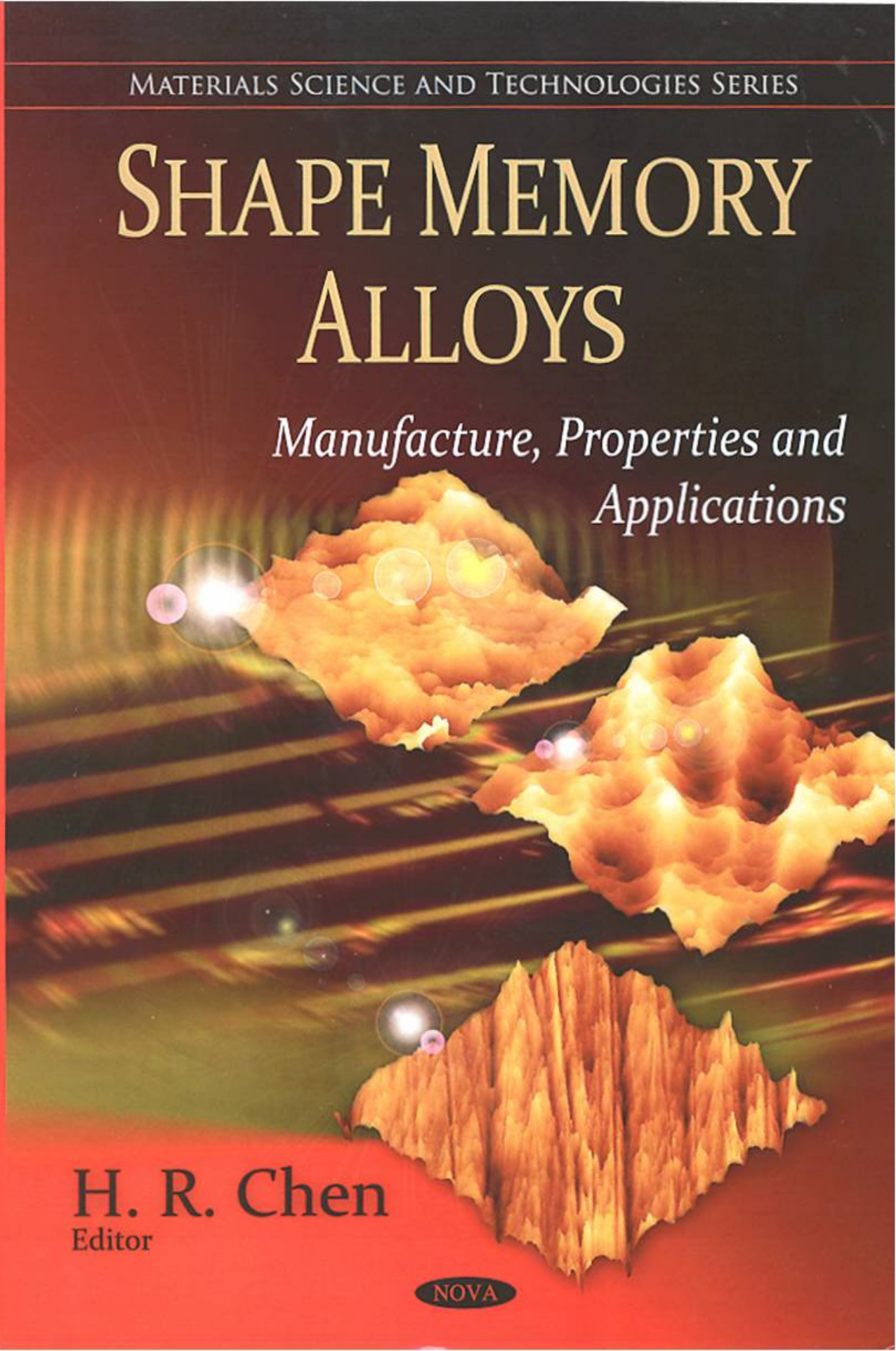

H. R. Chen
Editor

NOVA

In: Shape Memory Alloys
Editor: H. R. Chen, pp. 247-265

ISBN 978-1-60741-789-7

Chapter 8

EVOLUTION OF THE STRESS-INDUCED MARTENSITIC TRANSFORMATION IN A CUALBE SHAPE MEMORY ALLOY UNDER UNIAXIAL TENSION

F. M. Sánchez-Arévalo[1], G. Pulos[2] and R. Pérez-Cabeza de Vaca[3]
1 CCADET – Universidad Nacional Autónoma de México, A.P. 70-186, México D.F., C.P. 04510
2 Instituto de Investigaciones en Materiales, Universidad Nacional Autónoma de México, Apdo. Postal 70-186, Cd. Universitaria, México, D. F. C.P. 04510
3 Facultad de Ingeniería, Universidad Nacional Autónoma de México Apdo. Postal 70-186, Cd. Universitaria, México, D. F. C.P. 04510

ABSTRACT

The evolution of the stress-induced martensitic transformation was determined for a Cu-Al 11.2 wt%-Be 0.6 wt% shape memory alloy by digital image analysis. The CuAlBe tensile specimens were subjected to uniaxial tension; during the tension test, digital images of the polished and chemically etched surface's specimens were taken. From the tension test, the stress-strain curve representing the macromechanical behavior of the material was obtained. From the acquired images, the stress-induced martensitic transformation was observed and the number of grains, the area of the grains and the martensitic plates in the grains were estimated. Additionally, the orientation of the martensitic plates was determined for each image associated to the stress-strain curve.

Image analysis showed that, during the tension test, the martensitic variants appeared and disappeared due to the interaction between a grain and its neighbors, which is caused by the stress state of the grain, the original variant or variants, and the state of transformation of the neighboring grains. With the results from the micromechanical behavior, the strain measured with the strain gage could be resolved into its elastic and transformational components.

Introduction

Shape memory alloys (SMA's) are materials that can remember their original shape, after being elastically or pseudo-plastically deformed, by increasing their temperature. This behavior is useful in replacing conventional materials and develop new applications in science and daily life. The superelastic effect is one of the reasons there has been a continuous effort to understand, predict and explode the shape memory behavior of these materials.

The change of shape in shape memory alloys is due to a martensitic transformation. The martensitic transformation is defined as a first-order displacive process, where a body center cubic parent phase (austenitic phase) transforms by a shearing mechanism into a monoclinic or orthorhombic martensitic phase [1]. With this change of phase in the solid state other associated effects are present like the single shape memory effect, the double shape memory effect and the superelastic effect. All these effects are well known and they have been reported in literature [2-6].

The martensitic transformation has been observed in several classes of materials like metals, ceramics, polymers and in a biological structure [7]. Although the shape memory effect is present in almost all classes of materials, the metallic alloys with shape memory effects are preferred for developing new applications to replace conventional materials.

In this chapter, the behavior of a CuAlBe shape memory alloy under uniaxial tension is presented; in addition, a brief historical review of the research with the CuAlBe system is mentioned. The CuAlBe system appeared in 1982 and the first studies revealed that the system presented shape memory effects [8-10]. Since then, theoretical and experimental studies of the crystallography, microstructure, phase stability, thermomechanical and mechanical behavior as well as the micromechanical behavior have been carried out.

In 1997, Jurado *et al.*, worked on the order-disorder phase transition of the CuAlBe system [11]. Also in 1997, Hautcoeur *et al.* [12] determined the stress-temperature diagram for the CuAlBe system; in this diagram, they show the stability regions for the different types of martensite and determined the slope of transformation line. In 2000, Siredey and Eberhardt [13] studied the fatigue behavior of CuAlBe and showed that cyclic loading reduces the critical stress considerably. Balo, Ceylan and Aksoy studied, in 2001, the effect of deformation on the microstructure of CuAlBe [14, 15]; they reported that the addition of small quantities of Beryllium does not change the DO3 super-cell of the austenitic phase nor the martensitic 18R phase.

Trying to understand the mechanical behavior of SMA, Bouvet, Calloch and Lexcellent carried out a series of experiments using uniaxial and biaxial loading and determined the critical stress for two different compositions [16]; they used digital image correlation to check the boundary conditions for biaxial compression [17]. In 2004, Kaouache *et al.* studied the martensitic transformation in the superelastic regime for both monocrystal and polycrystal CuAlBe [18]; later on, in 2006 [19], they measured the crystalline orientation of three grains, determined the 24 variants present in CuAlBe and proposed a transformation criterion.

While in 1999, Siridey *et al.* proposed constitutive equations for SMAs at the grain level, no one had determined experimental strain fields in SMAs at the grain level. In 2006, Sanchez and Pulos [21] studied the stress-induced martensitic transformation and obtained displacement vector fields; recently, in 2008 [22], they obtained strain measurements averaged over several grains. Although several studies have been carried out to understand the CuAlBe

system, nobody had studied the evolution of the stress-induced martensitic transformation in a 2-D confined CuAlBe shape memory alloy using digital image analysis until now.

The objective of this chapter is to study the evolution of the stress-induced martensitic transformation in a CuAlBe shape memory alloy undergoing uniaxial tension. The grain size is comparable to the thickness of the sample so that the measured behavior on the surface is representative of the behavior throughout the thickness of the sample; on average, one grain spans the thickness of the sample and thus confinement of the grains occurs in two dimensions only. The behavior of the CuAlBe shape memory alloy is studied at the macro and micromechanical level. To understand the macromechanical behavior of CuAlBe, a uniaxial tension test was carried out using an MTS load frame; additionally, an optical microscope was attached to the load frame to reveal the micromechanical behavior of the material. The complete details are explained in the next section.

EXPERIMENT

To study the supereslastic effect, an austenitic alloy was elaborated. The composition was Cu-Al 11.2 wt%-Be 0.6 wt%, which is close to the eutectoidal composition [23]. An induction furnace (Leybold-Heraeus) was employed to elaborate the alloy by a melting process; this furnace has a controlled atmosphere and in our case argon gas was used. From the castings, suitable slices were cut and then hot rolled to obtain thin sheets. The length, width and thickness of the sheets were 280, 57 and 0.8 millimeters, respectively. These dimensions were reached after a 191 % hot-rolled (800 °C) deformation process. The hot-rolled process was carried out in an oven (Sola Basic-Lindberg model 847) and a roll machine (Fenn Amca International). Subsequently, the sheets were subjected to a heat treatment, called betatization, to reveal the shape memory effects; the sheets were heated at 750 °C during 15 minutes and then water-quenched to 95 °C during 20 minutes [21-25]. To determine the transformation temperatures, a differential calorimeter (TA Instrument model DSC 2910; USA) was used. This measurement was the first evidence that the shape memory effect in the CuAlBe alloy used in this study was present. From the sheets the uniaxial tension samples were cut in a numerically-controlled machine center; tensile specimens were obtained having a width of 3 mm, a thickness of 0.7 mm and an equivalent length[1] of 25.88 mm. The sample was polished and chemically etched with Ferric chloride ($FeCl_3$) to reveal the grains on the material's surface. The polished and chemically etched samples had a final thickness of 0.68 mm and were subsequently tested under uniaxial tension.

Tensile tests were carried out on a servohydraulic loading device (MTS 858 MiniBionix axial). To characterize the micromechanical behavior, an optical microscope was adapted to a high resolution digital camera –Nikon D2X 4288 × 2848 pixels– as shown in figure 2. The modular microscope works as an infinity-corrected compound microscope with magnifications of 10X. To control the MiniBionix MTS a 407 MTS controller was used while data and images were acquired with a National Instruments PXI-1002 system –including a 6281, 8331 and 4220 PXI-boards– and a PC. A virtual instrument (VI) was programmed in LabVIEW in order to synchronize and save the data and images. The virtual instrument was able to save the

[1] Length of a rectangular strip with the same width and thickness that would exhibit the same force-displacement behavior as the tensile specimen [26].

following parameters: time, displacement, force, strain and digital images. With the displacement, strain and force data, the macroscopic stress-strain curve was obtained and the acquired images were tagged to points in the stress-strain curve. Hence the micro and macro-mechanical behavior was determined simultaneously.

Image analysis was accomplished using a matlab scrip. The scrip consists in labeling objects or grains per image, the calculation of grains areas, (x, y) centroids of grains, the number of martensitic plates by grain and their orientation with respect to the cross-section area. From these results it was possible to determine the variants –groups of martensitic plates with the same orientation– that were induced by the applied loading; in addition, regions where martensitic plate reorientation occur were determined. The martensitic reorientation regions were analyzed in order to obtain the displacement vector field, strain measurements and the influence that neighboring grains have on the phase transformation.

With the series of images acquired during the tension test, displacement vector fields were calculated from pairs of images for each illumination type. The Willert and Gharib algorithm [28] was used to calculate $u_k(x_k, y_k)$ and $v_k(x_k, y_k)$, where u and v represent the displacements of an analysis object in the x and y directions respectively [26, 27]. The x and y represent the position coordinates of the analysis object in every image; subindex k indicates the corresponding object, which is defined as a 256x256 pixels area. The in-plane strains were determined by minimizing the errors of a six parameters linear model (typically used in linear elasticity theory) given by:

$$u_k(x_k, y_k) = A_1 x_k + B_1 y_k + C_1 + \delta_u(x_k, y_k) \qquad \text{Eq. (1a)}$$

$$v_k(x_k, y_k) = A_2 x_k + B_2 y_k + C_2 + \delta_v(x_k, y_k) \qquad \text{Eq. (1b)}$$

The minimization returns values for the A's, B's and C's where $A_1 = \varepsilon_x$ (strain in x direction), C_1= translation in x direction, $B_2 = \varepsilon_y$ (strain in y direction), C_2= translation in y direction. B_1 and A_2 are linear combinations of shear strain and rotation where the shear strain $\varepsilon_{xy} = (A_2+B_1)/2$ and the rotation $\theta = (A_2-B_1)/2$; $\delta_u(x_k, y_k)$ and $\delta_v(x_k, y_k)$ represent the (small) errors to be minimized

From the displacement vector field specific regions were selected to get the in-plane strains corresponding to those grains were the reorientation process occurred. The same analysis was done with the neighboring grains to observe the influence of neighbors on the phase transformation. Through image analysis the micro-mechanical behavior was determined separately from its macro-mechanical counterpart.

Results

The Cu-Al 11.2 wt%-Be 0.6 wt% shape memory alloy had the following transformation temperatures M_s= -95 °C, M_f=-103 °C, A_s=-91 °C and A_f=-76 °C, where M_s and M_f indicate the start and end of the direct transformation (austenite to martensite); A_s and A_f indicate the start and end of the inverse transformation (martensite to austenite).

The most important transformation temperature, for the superelastic effect (SE), is M_s because this temperature is related to the transformation (or critical) stress –usually denoted by

σ_c. The transformation stress denotes the point where the slope changes in the stress vs elongation ratio curve. The transformation stress and M_s are related by the Claussius Clapeyron equation as shown in equation 2 where T is the test temperature.

$$\sigma_c = 1.97MPa(T - M_s) \qquad \text{Eq. (2)}$$

Taking into account an M_s= -95 °C and employing equation 2, the transformation stress is around 230 MPa for the alloy's composition.

From the uniaxial tension test the superelastic effect can be observed in the stress vs elongation ratio curve, as shown in Figure 1. This effect is present when a material, in austenitic phase, is stressed until the martensitic phase appears in the material. The stress-induced martensitic transformation causes a reduction in the slope in the stress vs elongation ratio curve and represents the point when martensitic plates begin to appear. The slope in the martensitic region was not equal to zero, as expected, since the sample is a polycrystal [5].

In this case, an elastic deformation close to 0.23 % could be accommodated before the phase change started and due to the superelastic effect the deformation could be increased to 0.58 % without very little plastic deformation[2]. In addition, this curve showed the slope change starting around 240 MPa; furthermore, the theoretical transformation stress calculated from equation 2 and using M_s temperature is very close to the critical stress obtained from the uniaxial tension test. Using the first five data points –labeled A through E– and using a linear least-squares fit, the elastic modulus was estimated to be 114 ± 1 GPa.

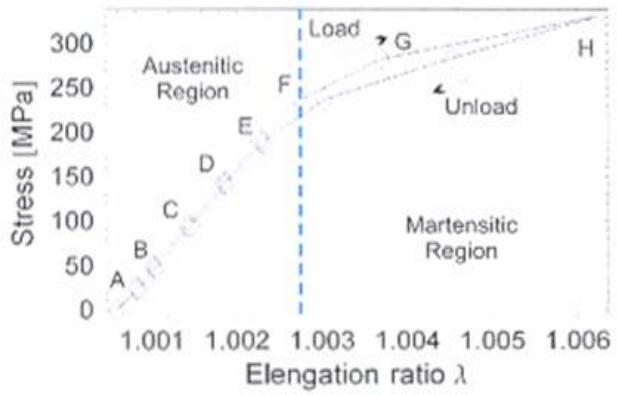

Figure 1. Stress vs elongation ratio curve.

The letters A to H in Figure 1, represent the state of stress and elongation ratio for each mosaic showed in Figure 2. The mosaics were obtained from an assembly of images that were acquired during the tensile test; each mosaic was constructed from six photographs and is 3890 x 12811 pixels. The mosaics in figure 2(a) to figure 2(h) show close to 100 grains in an area of 2.193 x 7.222 mm, which is the central part of the 3.01 x 14.00 mm test section; the area of the mosaic is roughly 38% of the test section –and considering an equivalent length of 25.9 mm, the mosaic represents 20.3% of the test sample. This number will later be used as a scaling factor to estimate the total number of plates in the test sample. The crystalline structure of the

[2] The accumulated plastic deformation can be estimated from the shift in the elastic return.

sample can be observed in these mosaics and the grain size could be determined; it was around 500 microns. As was mentioned earlier, from the grain size and the thickness of the sample, one can assume that the grains are confined only in the plane of the sample and that the measurements on the surface are representative of the through-the-thickness averages. Figures 2(a) to 2(e) show the sample in the austenitic phase. The austenitic phase presents a smooth (scratch-free) surface while the martensitic phase presents a roughness due to the growth of martensitic plates –which show up as dark lines or scratches due to the bright field illumination used– as it is shown in figures 2(f) to 2(h). From the mosaics, it is clear that the martensitic phase does not appear in all the grains in the region of study since the phase transformation depends on several factors such as stress level, crystalline orientation, test temperature, grain size and granular interaction, among others. Thus a more detailed and local analysis of a grain and its neighbors is needed to determine the micro-mechanics of the phase transformation.

As it was mentioned, the mosaics represent different snapshots of the phases present in the grains at different levels of stress in the sample. From figure 2(a) it is clear that the sample has the grains in the austenitic phase at 25 MPa. When the stress was increased, the martensitic phase began to appear at the top of the mosaics as shown the figures 2(b) trough 2(e) between 50 MPa to 190 MPa; nevertheless, the vast majority of grains have only the austenitic phase. From figure (2f) it is evident that the phase transformation has started since the martensitic plates show up in several grains.

In order to track the phase change and understand the micromechanical behavior, the grains were labeled as shown in Figure 3. This figure was used as a map of the transformation state during image analysis. As can be observed from Figure 3, the sample has 95 grains in the region of study, which is about the minimum number of grains needed to capture the macroscopic (averaged) mechanical behavior [29]; thus, the mosaic shows the minimum area required to do a representative study of the material.

A) 25 MPa B) 50 MPa C) 100 MPa D) 140 MPa

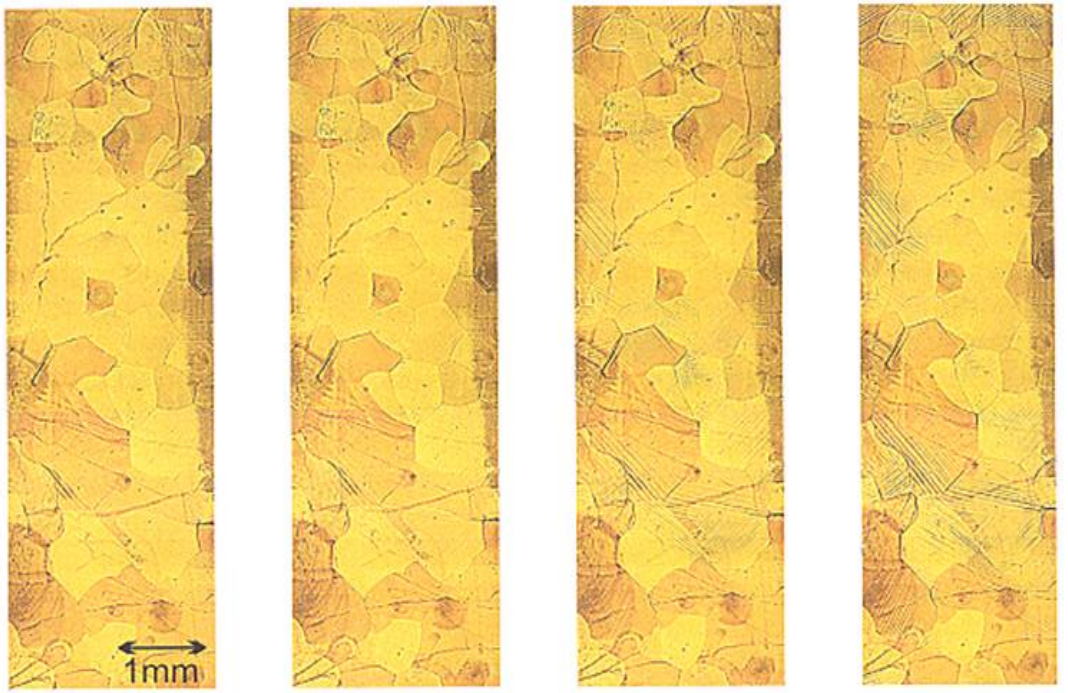

E) 190 MPa F) 240 MPa G) 280 MPa H) 330 MPa

Figure 2. Mosaics at different stress levels.

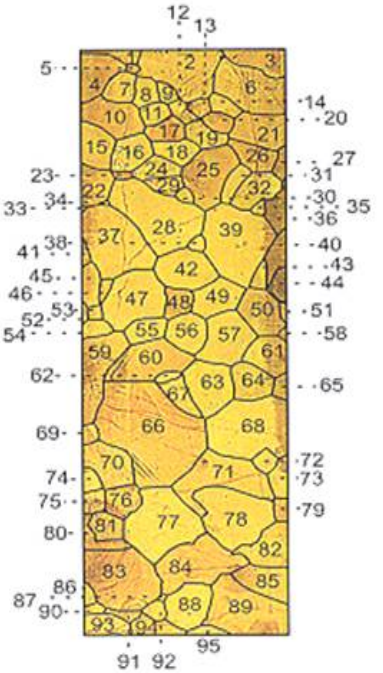

Figure 3. Labeled grains in the mosaics.

The labeling process of grains was done for all mosaics and the grain label was kept the same for each mosaic throughout the sequence. This analysis was able to reveal the transformational level of each grain. Figure 4 represents the evolution of the stress-induced martensitic transformation in each grain; the grain number, the number of martensitic plates and the stress level are represented in the x, y and z axis respectively. According to figure 3 the grain number goes from the top to the bottom of the mosaic; this grain number is plotted in the x axis in figure 4 and goes from left to right. From figure 4 it is also obvious that some grains at the top and bottom of the mosaic present martensitic plates at the initial stress level around 25 MPa; nevertheless, the central part of the mosaic does not present any grains with martensitic plates.

When the stress is increased, the number of martensitic plates increases including grains that had plates initially; the central part of the mosaic, that was free of the martensitic phase, begins to be covered with new plates.

The curves in red indicate that almost all grains are in austenitic phase and the curves in blue indicate that the previous relation has changed and now the majority of grains have undergone the change of phase (Austenite to Martensite). Although the number of plates increases as the stress is increased, there are cases in which plates disappear as the stress is increased. One such case is the grains 39-55 when the stress is increased from 50 to 100 MPa (last two orange curves). In this case, the peak –number of plates– at grain number 39 is reduced from three to two plates while the two plates in grain 47 disappear; in grain 55, the number of plates is reduced from four to three while the number of plates in grain 42 remains constant. There are other cases in which this happens but it serves as an example to point out the following: since the strain field must be compatible and a grain is surrounded by neighbors that may have different orientations and stiffness in the loading direction, the number of plates is not necessarily a monotonically increasing function of the stress. Plates may disappear or reappear in different orientations as the stress is increased even though, as it will be pointed out later, one can associate an increase in the transformational strain with each new plate. The increase in the transformational strain is the reason for the apparent plastic behavior –past the critical stress– of a shape memory alloy; the disappearance of the martensite plates, together with their associated reduction in transformational strain is the reason for superelastic unloading and recovery of the apparent plastic strains.

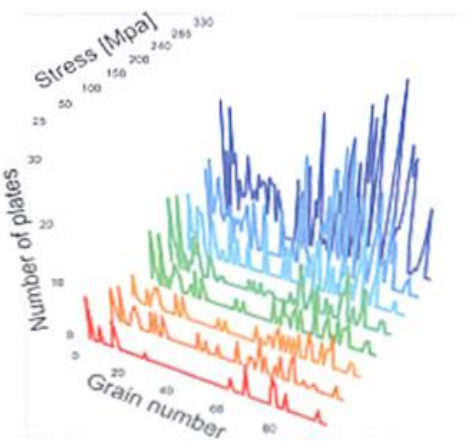

Figure 4. Evolution of the stress-induced martensitic transformation.

The stress vs. elongation ratio curve, presented in figure 1, shows a slope change due to the martensitic phase transformation. Now it is clear that there must be a representative percentage of the martensitic phase to observe that slope change. This change in figure 1 is also associated to the martensitic evolution curve marked in light blue in figure 4 –occurring at a stress level of 240 MPa. Thus observing, in the same figure, all the peaks in the curves at 240, 280 and 330 MPa, it could be assumed that the material presents a considerable percentage of the martensitic phase.

To quantify this percentage, all the grains with martensitic plates were taken into account from each mosaic and using the scaling factor that was defined earlier, the total number of plates in the sample can be estimated; in this case there were a maximum of 779 plates detected in the mosaic associated to 330 MPa. With a scaling factor of 1/0.203 = 4.93, the estimated maximum number of plates is 3840; the 41 plates detected in the mosaic at 25 MPa scale to an estimated 202 plates for the whole sample. The (total) number of plates as a function of stress is shown in figure 5.

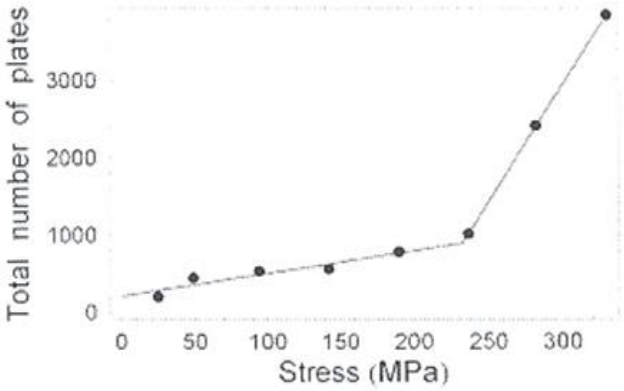

Figure 5. Total number of plates in the sample at different stress levels.

It should be noted that the (total) number of plates is a monotonically increasing function of stress –at least with the data that has been examined. Figure 5 shows an exponential growth of the martensitic plates where it is clear that the plates have grown suddenly, after 240 MPa, in different grains –and at different orientations. To characterize the number of plates as a function of stress, a (nonlinear) least-squares fit of a hyperbola was used; initially, a five parameter model was adjusted but the parameter associated to the radius of curvature of the hyperbola at its vertex[3] had a larger uncertainty than value and was eliminated. The four-parameter hyperbola is the union of its asymptotes, which are shown in the graph; the results of the fit are shown in table 1.

[3] The intersection of the asymptotes

Table 1. Four parameter hyperbolic fit

parameter	value	uncertainty	units
σ_c	233	4	MPa
plates @ σ_c	900	100	plates
slope before	2.9	0.5	plates/MPa
slope after	30	1	plates/MPa

The critical stress, σ_c, and the number of plates at the critical stress are the coordinates of the intersection of the asymptotes; the slopes represent the generation of plates before and after the critical point. Thus, martensite plates are generated at a rate of three for an increment of one MPa and this rate increases by a factor of ten after the critical stress is reached; two things should be noted: (1) martensitic plates are generated at stress well below the critical –or transition– stress and (2) the tenfold increase in the plate generation rate is has a direct effect in the sharp reduction of the (macroscopic) tangent modulus. In addition to the calculated parameters, the model was used to estimate the number of plates at zero load; the (residual) number of plates is 200 ± 70. This number matches well with the one obtained from a residual stress calculation that will be shown later.

From the image analysis the orientation of each martensitic plate was measured and arranged into groups or families using a simple threshold criterion; the criterion to define a group was a difference of 12 degrees between orientations. Using this criterion, the minimum and maximum number of groups was 3 and 210 at the lowest and highest stress level respectively (figure 6a and figure 6f). It should be pointed out that this criterion is somewhat arbitrary since the number of groups depends on the threshold –especially at the higher stresses; nevertheless, it is useful for presenting the data and it serves to detect the two main orientations present.

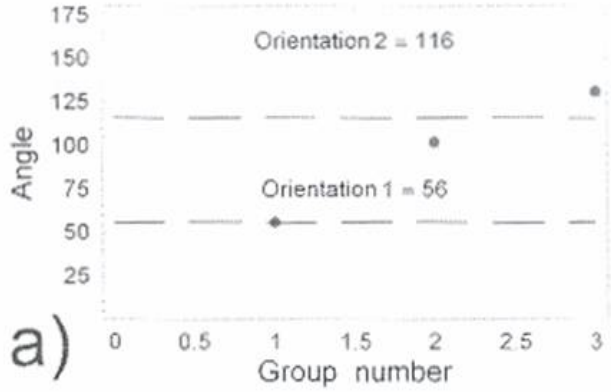

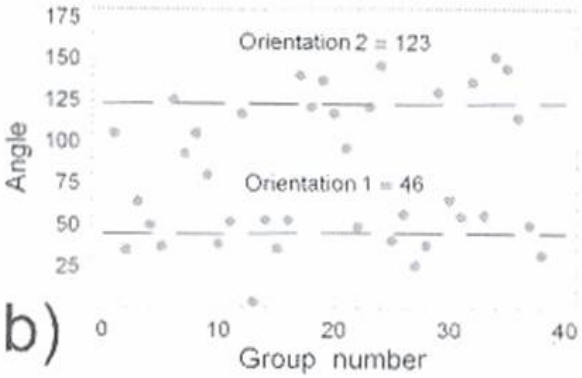
Orientation 2 = 123
Orientation 1 = 46
Angle
Group number
b)

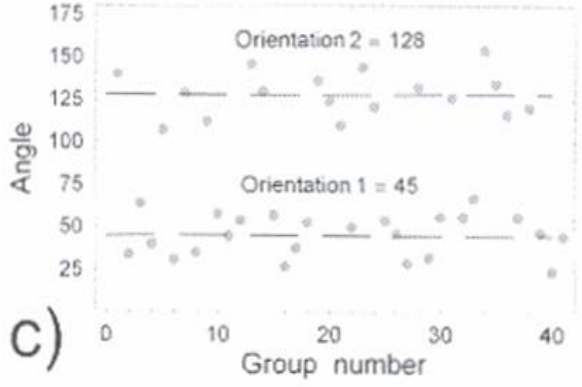
Orientation 2 = 128
Orientation 1 = 45
Angle
Group number
c)

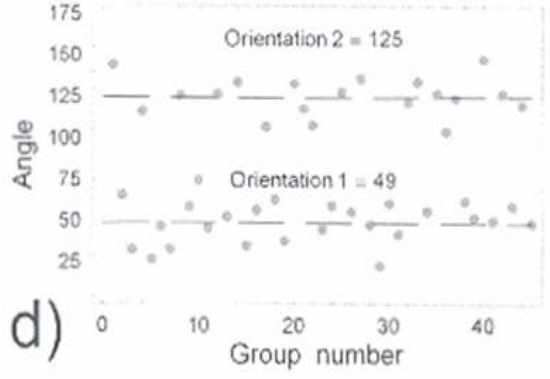
Orientation 2 = 125
Orientation 1 = 49
Angle
Group number
d)

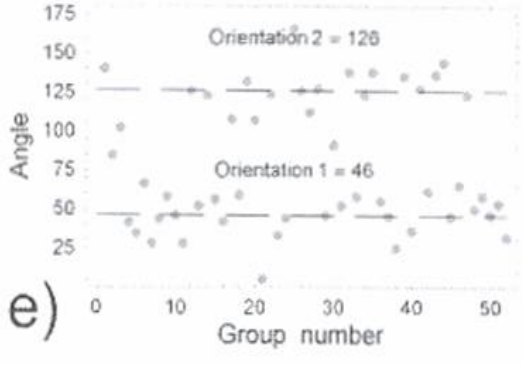
Orientation 2 = 126
Orientation 1 = 46
Angle
Group number
e)

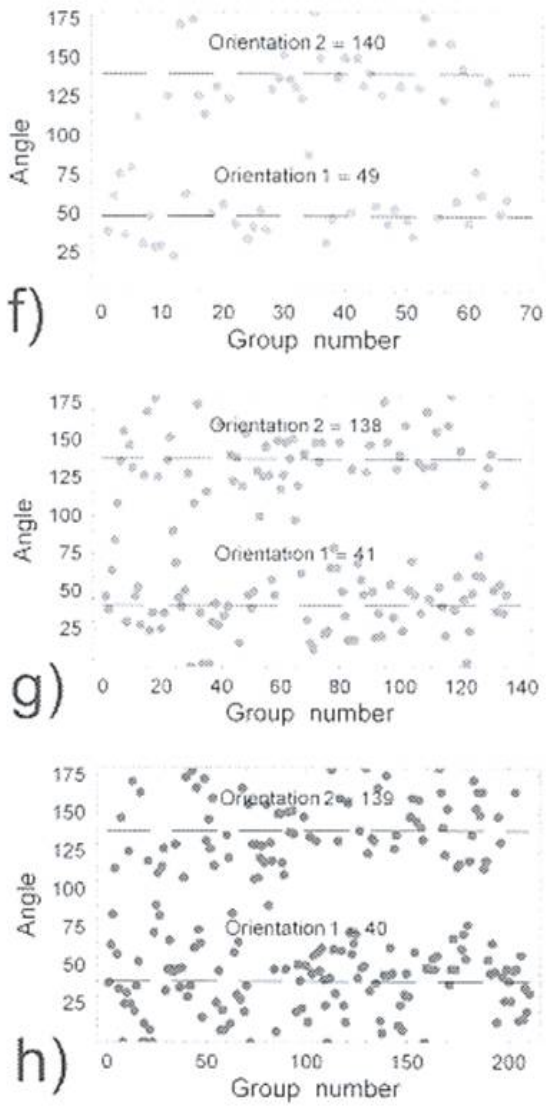

Figure 6. Stress-Induced orientation distribution due to the applied force direction and grain geometry.

Figure 6 shows the angle vs. the number of groups for all mosaics; two main orientations can be detected. The first one corresponds to a range between 25 and 75 degrees while the second one to a range between 10 and 160 degrees. The clustering of the groups is centered around the angles of maximum shear stress, which in the case of uniaxial tension are 45 and 135 degrees. The averages of the clusters are shown in the figures. The evolution of orientations presented in figure 6 shows that clustering is somewhat dynamic since it is easier to detect it for some of the stress levels but seem to disappear for some others. Clustering at 100 MPa is easier to detect than the clustering at 50 MPa or at the higher stress levels; for the last two stress levels, clustering occurs for the larger group numbers which are groups associated with larger grain numbers that correspond to grains at the bottom of the mosaics.

As it was pointed out earlier, plate formation depends, among other things, on the stress level, the grain geometry and the neighboring grains; the orientation also depends on which of

variants in the cell is activated. CuAlBe has the D03 cell, which has 24 variants; grain orientation and loading direction are critical factors to determine which of the variants is activated but at higher stress levels, it may be possible to activate many of the variants. The end effect of this complex problem is the evolution of orientations presented in figure 6.

Although predicting or analyzing the orientation of martensite plates is a very complex problem, tracking the number of plates generated can be used to split the total strain into an elastic component and a transformational one. If one assumes that each plate generates a given amount of transformational strain, the macroscopically measured total strain can be divided into the elastic response of the austenite phase and the additional (transformational) strain that comes from the phase change. Thus,

$$\sigma = E_A \varepsilon_e + \sigma_0 \qquad \text{Eq. (3a)}$$

$$\varepsilon_T = \varepsilon_e + \varepsilon_{AxM} = \varepsilon_e + \alpha \text{plates}[\sigma] \qquad \text{Eq. (3b)}$$

where σ is the stress, E_A is the elastic modulus of the austenite phase, ε_e is the elastic strain, σ_0 is the residual stress, ε_T is the total strain, ε_{AxM} is the transformational strain, α is the constant of proportionality and the number of plates as a function of stress is the fitted hyperbola found before. The results of the analysis are shown in table 2.

Table 2. Elastic and transformational strain fit

parameter	value	uncertainty	units
E_A	176	3	GPa
σ_0	39	1	MPa
α	1.03	0.01	□□/plate

The elastic modulus is higher than the one obtained from the strain gage measurements (114 ± 1 GPa); it is clear that this should be the case since there is some plate generation occurring before the critical stress is reached. The residual stress calculated is equivalent to 220 ± 10 $\mu\varepsilon$, which can be converted into some 210 ±10 residual plates; this measurement is comparable to the previous estimate of 200 ± 70 plates.

The proportionality constant of 1.03 ± 0.01 $\mu\varepsilon$/plate has a small uncertainty since the calculated plate function, shown in figure five, has the same form as the macroscopic behavior shown in figure 1; the only data point which does not fit the analysis is the one labeled "G", which has a smaller strain than the expected value. In this case, the difference in strain is about 770 $\mu\varepsilon$; this strain is very large compared to the standard deviation of the analysis and was not used in the calculations. The results are summarized in figure 7, which shows the elastic behavior (blue) that characterizes the austenite phase and the transformational strain (green) that is 1.03 times the plate function that was shown in figure 5. The addition of these two strain models the total strain vs stress behavior that was shown in figure 1; in the plot, the datum that was labeled "G" is shown together with the predicted one "G'."

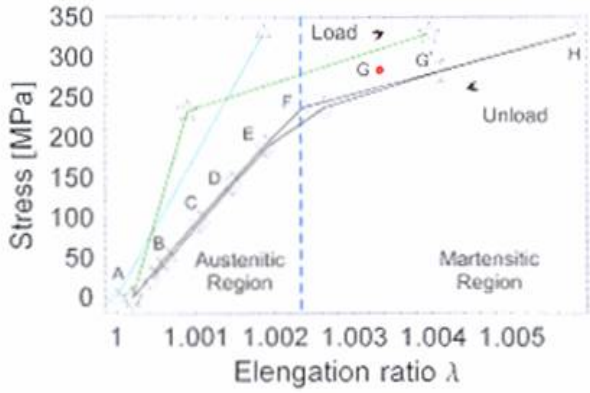

Figure 7. Elastic, transformational and total strain as a function of stress

Using these results, one can compare the elastic, transformational and total strains with the ones obtained from local image analysis. Since granular interaction plays an important role in the evolution of the transformation phase, three different regions of the mosaic were selected at different stress levels. To study the granular interaction of these regions two images per region were selected as shown in figure 8a and 8b for the first region, figure 8d and 7e for the second one and figure 8g and 8h for the third one. The arrow next to figure 8a indicates the loading direction.

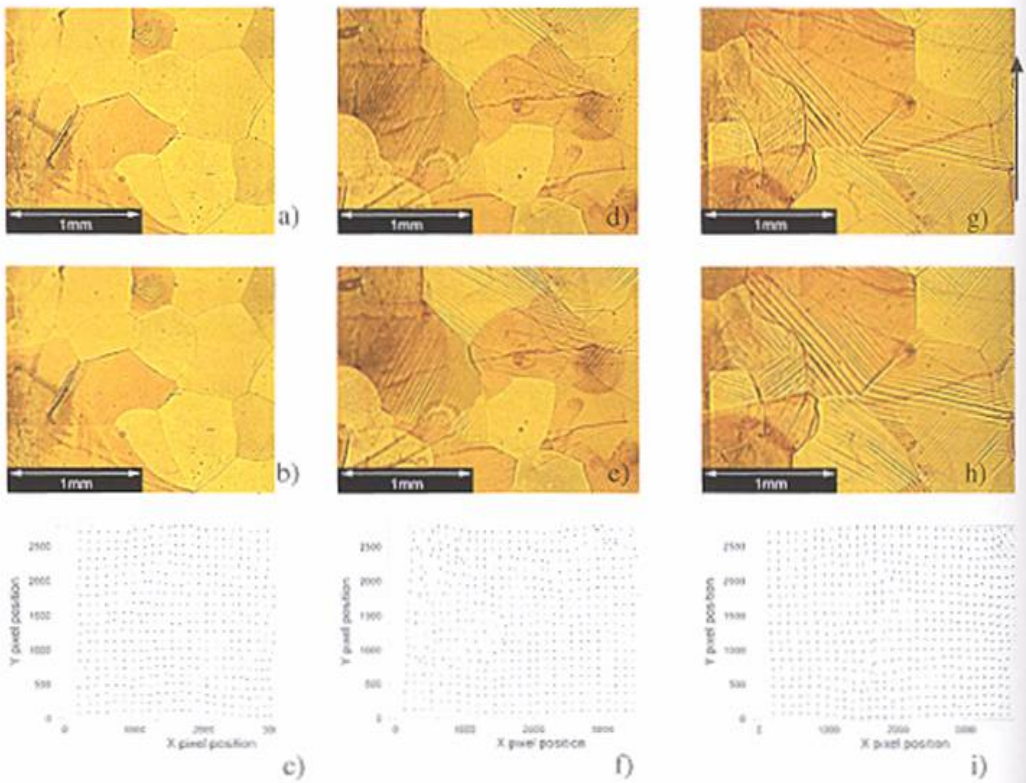

Figure 8. Granular interaction observed with displacement vector fields

One of the three cases selected comes from data before the critical stress is reached (austenite loading range) while the other two are cases taken after the critical stress was reached; of the two later cases, one is from a region that has lower plate density while the last one come from a region that ends up with a high plate density. From each pair of images the displacement vector field was calculated using the Willert and Gharib algorithm [28]. The images in figure 8a and 8b correspond to the central part of the mosaic. These images showed that almost all grains, except the grain labeled with the number 60 in figure 3, were in austenitic phase; a smooth hyperbolic vector field was obtained. The last pair of images showed that all grains were in martensitic phase as it is shown in figure 7g and 7h; in this case, the displacement vector field obtained from them was not a smooth hyperbolic field. For the second and third cases, figures 8f and 8i showed disturbances in some sectors of the displacement field. Although one may argue that the disturbances are due to the granular interaction caused by the growth of martensitic plates, the main assumption in the calculation of the displacement vector field is violated. As it was pointed out before, to obtain a displacement vector field, two images –from two different loads– are compared; the second image is assumed to be the first one except that it has been stretched or deformed. When new plates appear in the second image, which are not in the first one, the main assumption in the calculation is violated and the results become unreliable. This fact can be illustrated when the strains calculated from the displacement field are compared with the macroscopic strain calculations; these results are shown in table 3.

Table 3. Local and global strain calculations

Case	Stress increment (MPa)	Total strain from strain gage ($\mu\varepsilon$)	Local strain from DIC ($\mu\varepsilon$)
C to D	40 ± 10	300 ± 100	350 ± 10 + ??
G to H	50 ± 10	1800 ± 400	2300 ± 100 + ??
G to H	50 ± 10	1800 ± 400	10, 100 ± 200 + ??

For the first case (C to D) both calculations coincide; the actual reading from the strain gage was 346 $\mu\varepsilon$ but it was rounded off to 300 due to the large uncertainty. The large uncertainty comes mostly from the uncertainty in the stress increment, which is large since the stress increment is small although the uncertainties in the stresses are about 5%. The strain from the DIC calculation was 354 $\mu\varepsilon$, which was rounded to 350; there is a missing uncertainty that comes from the calculation of the displacement field but the uncertainties could not be extracted from the software that was used.

For the second case, which has stresses larger than σ_c, the strains are much larger since (martensite) plates are generated at ten times the rate below σ_c; within the give uncertainties, both results coincide. This case was taken from a region that was relatively free of plates. In the last case, which has images full of plates, the calculated strain from DIC is unrealistically high; the reason may be that the main assumption –comparing the same image– is clearly violated since there are more plates in image 8h than there are in image 8g.

To determine if the DIC strain calculation could be extended to the grain level, the best case (C to D) was selected and the image that was shown in figure 8b was superposed with the displacement vector field (figure 8c). The grain boundaries were used to select the displacement vectors located at those grains; thus, individual grains were isolated and

processed. The grains selected were labeled in figure 3 with the following numbers 55, 56, 57, 60, 61, 62, 63 and 64. The colored displacement field vector is shown in figure 9.

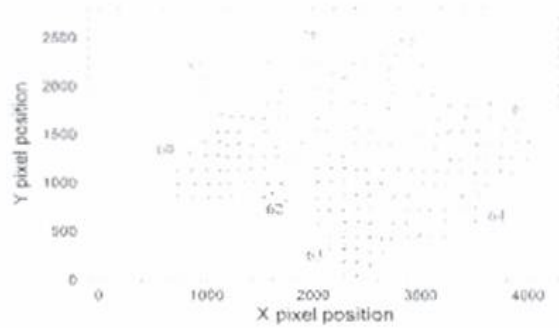

Figure 9. Displacement vectors for each grain by colors.

Using this data, the longitudinal strain for each grain was calculated with equations 1a and 1b. The resulting strains –named longitudinal strain to indicate that it is the strain in the loading direction– are plotted in figure 10; the levels of the elastic (blue), transformational (green) and total strains are also shown in figure 10.

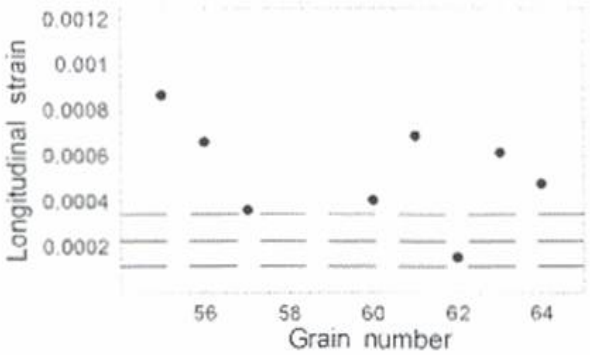

Figure 10. Longitudinal strain per grain.

Uncertainties are not shown in figure 10 since they could not be obtained for the displacement field calculation; narrowing down the selection of vectors corresponding to a single grain show that there is a tendency towards inhomogeneous strain at the grain level. These microscopic calculations yield similar results that the (macroscopically) calculated total strain. Clearly, higher resolution and the uncertainties from DIC are needed to characterize further the strain field at the grain level.

Conclusion

The evolution of the stress induced martensitic transformation was characterized by tracking the number of martensite plates that appeared –and some times disappeared– during a uniaxial test of a CuAlBe SMA alloy. A critical stress of 233 ± 4 MPa was obtained and the rates of plate generation before and after the transition were also determined.

It was observed that martensite plates are generated at stresses well below the critical one, although the generation rate is only 10% of the rate of plate generation past the critical stress. The sharpness of the transition could not be determined since the uncertainty in the parameter related to the radius of curvature had an uncertainty much larger than its value; in this case the hyperbola mapped onto its asymptotes, which was the function used to determine (martensite) plate generation as a function of stress. Having this function similar in shape to the macroscopic stress-strain behavior allowed us to make the key assumption that the transformational strain is proportional to the number of plates, which in turn allowed us to separate the total strain into its elastic and transformational components. With this analysis, the elastic modulus of the austenite phase and the constant of proportionality were determined. A better assumption may be that the transformational strain is proportional to the volume fraction of the transformed phase; however, counting the number of plates in each of the mosaics may be useful to estimate the transformational strain if the area examined is comparable to the area of the sample.

Comparison between macroscopic and microscopic strain calculations was in agreement for cases where there were a small number of plates in the images; in the case where the two images have a large –and different– number of plates, the results from the microscopic calculation yield unrealistically high strain. Extending the calculation to individual grains showed inhomogeneous strains but more resolution and known uncertainties are needed to determine the strain field down to the grain level.

ACKNOWLEDMENTS

This work was developed with financial support from the PAPIIT DGAPA-UNAM program through grants IN100706, IX121504 and from CONACyT through grants P47758212 and NC204. UNAM CTIC-DGAPA provided a postdoctoral fellowship for F.M.S.A. and additional resources were provided by the ICyTDF program (Instituto de Ciencia y Tecnologia del Distrito Federal). The authors are grateful to Luis A. Ferrer and Mario Acosta for the use of the electrical strain gage equipment and to Gabriel Lara for his technical support.

REFERENCES

[1] Olson, M.; Cohen, G. B.; Clapp, P.C. On the classification of displacive phase transformations. *Proceedings of the international conference on martensitic transformation. ICOMAT 79*, Cambridge-Massachussets U.S.A. 1979 pp. 1-11.

[2] Patoor, E.; Berveiller, M. *Les alliages à mémoire de forme. Technologies de pointe*; Hermes, PARIS, 1990 ; pp 09-63.

[3] Wayman, C. M.; Duerig, T. M. *An introduction to martensite and shape memory, Engineering Aspects of Shape Memory Alloys.* Butterworth-Heinemann, London (UK), pp. 3-20.

[4] Otzuka, K.; Wayman, C. M.; Nakay, K.; Sakamoto, H.; Shumizu K. *Acta Metallurgica*, 1976. Vol.24, pp. 207-226.

[5] Yang, J. H.; Wayman, C. M. *Mater. Charact.* 1992. vol 28, pp. 23-35.

[6] Yang, J. H.; Wayman, C. M. *Mater. Charact.* 1992,vol. 28, pp. 37-47.

[7] Czichos, H. "Adolf Martens and the research of martensite." *Proceedings of the european conference on martensitic transformation in science and technology*. Bochum, Alemania, 1989; pp. 3-14.

[8] Higuchi, A.; Suzuki, K.; Matsumoto, Y.; Sugimoto, K.; Komatsu, S.; Nakamura, N. "Shape memory effect in Cu-Al-Be ternary alloy." In: *Proceedings of the international conference on martensitic transformations*, ICOMAT 1892. Leuven, Belgica. pp. 767-772.

[9] Higuchi, A.; Suzuki, K.; Sugimoto, K.; Nakamura, N. "Thermal stability of Cu-Al-Be shape memory alloy." In: *Proceedings of the international conference on martensitic transformations*. ICOMAT 1896. Nara, Japan. pp. 886-890.

[10] Belkahla S.; Flores H.; Guenin G. *Mater. Sci. Eng. A-Struct. Mater. Prop. Microstruct. Process.* 1993, A169. p. 119-124.

[11] Jurado, M.; Castan, T.; Mañosa, L.; Planes, A.; Bassas, J.; Alcobe, X; Morin, M. *Philos. Mag.* 1997, Vol. 5. pp. 1237-1250.

[12] Hautcoeur, A.; Eberhardy, A.; Patoor, E.; Berveiller M. "Thermomechanical behavior of monocrystalline Cu-Al-Be shape memory alloys and determination of the metastable phase diagram." *Journal de physique IV. Colloque C2, suplément au Journal de Physique III*.1995,Vol. 5. pp. c2-459 to c2-464.

[13] Siredey, N.; Eberhardt, A. *Mater. Sci. Eng. A-Struct. Mater. Prop. Microstruct. Process.*, 2000, A290, pp. 171-179.

[14] Balo, N.; Ceylan, M.; Aksoy, M. *Mater. Sci. Eng. A-Struct. Mater. Prop. Microstruct. Process.* 2001, A311, pp. 151-156.

[15] Balo, N.; Ceylan M. *J. Mater. Process. Technol.* 2002 Vol. 124. pp. 200-208.

[16] Bouvet C.; Calloch S.; Lexcellent, C. *Transactions of ASME.* 2002,Vol 124. pp. 112-124.

[17] Chevalier, L.; Calloch, S.; Hild, F.; Marco, Y. Eur. *J. Mech. A/Solids*. 2001, vol. 20. pp. 169-187.

[18] Kaouache, B.; Berveiller, S.; Inal, K.; Eberhardt, A.; Patoor, E. *Mater. Sci. Eng. A-Struct. Mater. Prop. Microstruct. Process.* 2004, A378. pp. 232-237.

[19] Kaouache, B.; Inal, K.; Berveiller, S.; Eberhardt, A.; Patoor, E. *Mater. Sci. Eng. A-Struct. Mater. Prop. Microstruct. Process.* 2006, A 438-444. pp. 773-778.

[20] Siridey, N.; Patoor, E.; Berveiller, M.; Eberhardt, A. Int. J. Solids Struct. 1999, Vol. 36 pp. 4289-4315.

[21] Sánchez, F. M.; Pulos, G. *Materials science Forum*. 2006,Vol. 509. pp. 87-92.

[22] Sánchez-Arévalo, F. M.; Pulos, G. *Mater. Charact.* 2008,Vol. 59. Issue 11. pp. 1572-1579.

[23] Belkahla, S. "Elaboration et caracterisation de nouveaux allieages á mémoire de forme basse température type Cu- Al-Be." Ph. D. Thesis.1990, Inst. Nat. Sc. Appl., Lyon France. Pp 132.

[24] Belkahla, S. Dégration thermique de l'effet mémoire de forme d'un alliage ternaire: Cu-Zn-Al *These de magister en phisyque des matérriaux*. Université d'Annaba (Algérie) 1985, pp. 87.

[25] Flores, H.. "Stabilite thermique de la phase _ et de l'effet memoire double sens d'un alliage a memoire de forme du type Cu-Al-Be." Ph. D. Thesis.1993, Inst. Nat. Sc. Appl., Lyon France. Pp 150.

[26] Sánchez-Arévalo, F. M. "Estudio experimental del comportamiento mecánico de un material con memoria de forma." Ph. D. Thesis. 2007, Universidad Nacional Autónoma de México. México. pp 90.

[27] Chu, T. C.; Ranson, W. F.; Sutton, M.A.; Peters, W.H. *Exp. Mech.*. 1985, 25(3). pp. 232-244.

[28] Willert, C. E.; Gharib, M. *Exp. Fluids*. 1991,Vol. 10. pp. 181-193.

[29] Nygards, M. *Mech. Mater*. 2003. Vol. 35. pp. 1049-1057.